 CMES, vol.73, no.3, pp.267-298, 2011

Multiple Damage Detection Method for Beams Based on Multi-Scale Elements Using Hermite Cubic Spline Wavelet

Jiawei Xiang[1,2] **and Ming Liang**[1, 3]

Abstract: The importance of damage detection in **structures** has been widely recognized in mechanical and civil engineering. A new method is proposed to detect multiple damages based on frequency measurement. According to linear fracture mechanics theory, the damages are modeled by rotational springs. The first problem of interest is concerned with the construction of multi-scaling wavelet finite element model using Hermite cubic spline wavelet on the interval (HCSWI) in the forward problem analysis to obtain damages detection database. The second problem is the inverse problem analysis to determine the number of damages, their locations and depths based on the minimum Root-mean-square (RMS) of the differences between the measured and the computed frequencies. The performance of the proposed method has been verified by numerical examples and experimental study of two-damage cantilever beam.

Keywords: Multiple damage detection Hermite cubic spline wavelet on the interval Multi-scale wavelet-based element

1 Introduction

Damages often occurs on structures and may cause catastrophic failures. Structural health monitoring has been receiving increasing interest in both academia and industry for several decades. There has been numerous of research focusing on model-based methods for damage detection in structures during recent years. The model-based damage detection method involves two kinds of problems, one is the forward problem analysis used to obtain damage detection database for struc-

[1] Department of Mechanical Engineering, University of Ottawa, 770 King Edward Avenue, Ottawa, Ont., Canada K1N 6N5

[2] School of Mechanical and Electrical Engineering, Guilin University of Electronic Technology, Guilin, Guangxi, P.R.China, 541004

[3] Corresponding Author: Ming Liang, E-mail: liang@eng.uottawa.ca

tures using finite element method (FEM), the other is the inverse problem analysis to seek optimized value from damages detection database using surface fitting technique (Owolabi, et al., 2003), genetic algorithms(GAs) (He, et al., 2001), neural networks(NNs) (Wu, et al., 1992) or others. The research in the past few decades on cracked structures and rotors is well documented in a review paper by Wauer (Wauer, 1990) ,surveys on beam-like structures by Dimarogonas (Dimarogonas, 1996) and Doebling (Doebling, et al., 1998) and more recently by Montalvão (Montalvão, et al., 2006). The model-based methods have definite advantages in applications for underwater platforms, bridges, wind turbine blade, etc. In such cases, inspections with a portable instrument, can be carried out, to measure the response under environmental excitation. If this excitation is considered to be white noise, the response of the structure will be, to a certain scale, the transfer function (can be used to measure the natural frequencies) of the structures. Therefore, this method may provide reasonable results in many fields.

A significant amount of research involving the prediction of the response of structures to the presence of a transverse crack or damage. The detection of transverse cracks by the application of the linear fracture mechanics theory. In order to evaluate the local flexibility or stiffness introduced by the damage, neglecting the effects that may be incorporated into the mass and damping matrices. The thrust of the most works in the past has been on a structure with a single transverse surface damage (Dimarogonas, 1996;Doebling, et al., 1998; Montalvão, et al., 2006). Recently, a high performance wavelet-based finite element method was proposed to detect one damage in beams and shafts (Xiang, et al., 2006; 2007; 2008). However, when more than one damage appears in structures, the dynamic response becomes more complex depending upon the damage parameters (locations and depths of these damages). The multiple damage effects and identification methods are reviewed by Sekhar (Sekhar, 2008). While most of the studies dealing with multiple damage method is only address the forward problems, i.e. determination of natural frequencies or modal shapes using traditional finite element method (Patil and Maiti, 2003; Perera and Ruiz, 2008; Lee, 2009a; 2009b; Khiem and Lien, 2004). To obtain a more precise damage detection database for the inverse problem solutions in damage detection procedures, numerously traditional finite element elements are needed.

Neural networks(NNs) is a useful tool to deal with inverse or pattern recognition problems in engineering. Various researchers have started to experiment with NNs for damage identification purposes during the last decade (Liu, et al., 2002; Zachiarias, et al., 2004; Yuan, et al., 2005; Lee, et al., 2005). However, the application of NNs to multiple damage detection has been very limited mainly due to the slow process to obtain the optimal damage parameters from a large number of train-

ing samples. Multiple damage detection is a difficult task. If there exist n damages in structures, $2n$ damage parameters(n damage locations and n damage depths) will be detected and at least $2n$ frequencies (Dilena and Morassi,2009; 2010; Morassi, 2007; Gaddemi and Morassi, 2007) are needed to accomplish this task. Therefore, in the present model-based multi-damage detection methods, the combination of FEM with frequency ratio method is commonly used and at least four frequencies are needed to detect two damages. However, the traditional finite element method can not work well to get a satisfactory detection results. Then, a dynamic mesh-refinement method (DMRM) of multiple damage detection is presented by using single scale wavelet finite element method (Chen, et al., 2006).

The wavelet numerical methods, which have been developed in recent years, can be viewed as a method in which the approximation functions are defined by the scaling or wavelet functions, similar to those used in signal and image processing (Libre, et al., 2008; 2009; Yan, et al., 2008). And the wavelet-based numerical method has two prominent advantages. One is to upgrade scale to obtain the scaling functions at different scale that can be employed directly to form the multi-scale approximation bases. The other is to hierarchically approximate using the lifting relationship between scale and wavelet spaces. Therefore, the wavelet method is well argued by many researchers in various fields and the results show that wavelet approximation can reduce the computation and storage costs (Ma, et al., 2003; Chen, et al., 2004; Chen, et al., 1995; 1996a; 1996b; Han, et al., 2006; 2007; 2009; Zhou and Zhou, 2008a; 2008b; Diaz, et al., 2009; Vampa, et al., 2010).

The purpose of the present work is to establish a method for predicting the locations and depths of multiple damages in beam-like structures by considering several lowest frequencies of the damage structures. We combine the multi-scale wavelet-based finite element method using HCSWI with a simple minimal value determination method using root-mean-square (RMS) to make an effective and accurate detection in multi-damage structures. The influence of damage parameters on changes of several lowest frequencies are discussed by numerical simulation. Some experimental works to detect two damages in cantilever beam testify the present method.

2 Multi-scale Wavelet-based finite element method

2.1 Wavelet bases of Hermite cubic splines on the interval

Classical approaches to wavelet construction deal with multiresolution analysis (MRA) on the entire real space $\mathbf{R}$ and the corresponding wavelets are often defined on the entire square integrable real space $L^2(\mathbf{R})$. Therefore, the numerical instability phenomenon will occur when the wavelets are employed as interpolating functions for numerical simulation (Jia and Liu,2006). Wavelets defined on the

interval will overcome this problem. In this study, the wavelet bases of Hermite cubic splines on the interval are employed as the interpolating functions to construct multi-scale wavelet-based beam element for analyzing damaged beam-like structures.

Here we denote $L^2(\mathbf{R})$ as the linear space of all square integrable real valued functions on $\mathbf{R}$. The inner product in $L^2(\mathbf{R})$ is defined as $< u,v >:= \int_{\mathbf{R}} u(x)v(x)dx$, $u,v \in L^2(\mathbf{R})$. If $< u,v >= 0$, we say that u and v are orthogonal. The norm of a function f in $L^2(\mathbf{R})$ is given by $\|f\|_2 := \sqrt{< f,f >}$.

Let ϕ_1 and ϕ_2 be the cubic splines supported on the interval [0, 1], given by

$$\phi_1(x) := \begin{cases} (1+x)^2(1-2x) & for \quad x \in [-1,0], \\ (1-x)^2(1+2x) & for \quad x \in [0,1], \\ 0 & for \quad others, \end{cases} \tag{1}$$

and

$$\phi_2(x) := \begin{cases} (1+x)^2 x & for \quad x \in [-1,0], \\ (x-1)^2 x & for \quad x \in [0,1], \\ 0 & for \quad others, \end{cases} \tag{2}$$

The graphs of ϕ_1 and ϕ_2 are depicted in Fig.1. Clearly, both ϕ_1 and ϕ_2 belong to $C^1(\mathbf{R})$.

The corresponding wavelets ψ_1 and ψ_2 supported on the interval [-1, 1] are (Jia and Liu, 2006)

$$\begin{cases} \psi_1 = -2\phi_1(2x+1) + 4\phi_1(2x) - 2\phi_1(2x-1) - 21\phi_2(2x+1) + 21\phi_2(2x-1), \\ \psi_2 = \phi_1(2x+1) - \phi_1(2x-1) + 9\phi_1(2x+1) + 12\phi_2(2x) + 9\phi_2(2x-1). \end{cases} \tag{3}$$

They satisfy the conditions $< \psi_1{}', \phi_m{}'(\bullet - j) >= 0$ and $< \psi_2{}', \phi_m{}'(\bullet - j) >= 0, \quad m = 1,2, \forall j \in \mathbf{Z}$, and their shifts generate the wavelet space W. Fig.2 shows the graphic of ψ_1 and ψ_2. ψ_1 is symmetric and ψ_2 is antisymmetric.

The above mentioned wavelets can generate a wavelet basis for space $H_0^1(0,1)$. Therefore, we have the following decomposition of $H_0^1(0,1)$:

$$H_0^1(0,1) = V_1 + W_1 + W_2 + \cdots, \tag{4}$$

where V_1 is the scaling space and W_n for $n = 1,2,\cdots$ is the wavelet space at differential levels.

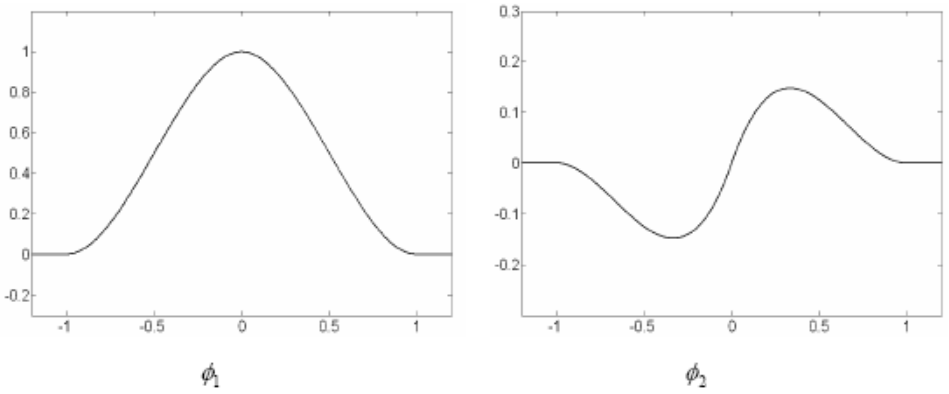

Figure 1: Hermite cubic splines on **R**

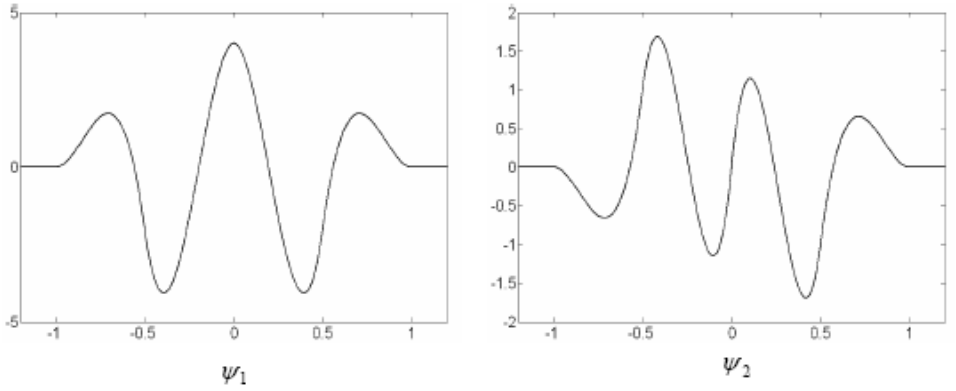

Figure 2: Wavelets $\psi_1 and\ \psi_2$

Define the scaling functions $\phi_{1,k}$ as

$$\begin{cases} \phi_{1,1}(x) := \sqrt{\dfrac{5}{24}}\phi_1(2x-1), \\ \phi_{1,2}(x) := \sqrt{\dfrac{15}{4}}\phi_2(2x), \\ \phi_{1,3}(x) := \sqrt{\dfrac{15}{8}}\phi_2(2x-1), \\ \phi_{1,4}(x) := \sqrt{\dfrac{15}{4}}\phi_2(2x-2), \end{cases} \tag{5}$$

and the wavelets $\psi_{n,k}$ as

$$\begin{cases} \psi_{n,k}(x) := \dfrac{2^{-n/2}}{\sqrt{729.6}}\psi_1(2^n x - \dfrac{j}{2}) \quad for \;\; j = 2,4,\cdots,2^{n+1}-2, \\ \psi_{n,k}(x) := \dfrac{2^{-n/2}}{\sqrt{153.6}}\psi_2(2^n x - \dfrac{j-1}{2}) \quad for \;\; j = 1,3,\cdots,2^{n+1}-1, \\ \psi_{n,1}(x) := \dfrac{2^{-n/2}}{\sqrt{76.8}}\psi_2(2^n x), \\ \psi_{n,2^{n+1}}(x) := \dfrac{2^{-n/2}}{\sqrt{76.8}}\psi_2(2^n x - 2^n). \end{cases} \tag{6}$$

All the scaling functions $\phi_{1,k}$ and wavelets $\psi_{1,k}$ on the interval $[0,1]$ are shown in Fig.3. Suppose $u \in V_1$ and $v_n \in W_n$ for $n = 1,2,\cdots$, the wavelets have a useful property that each wavelet at different levels is orthogonal with respect to the inner product, i.e. $< u', v_n' >= 0$ for all n and $< v_m', v_n' >= 0$ for $m \neq n$.

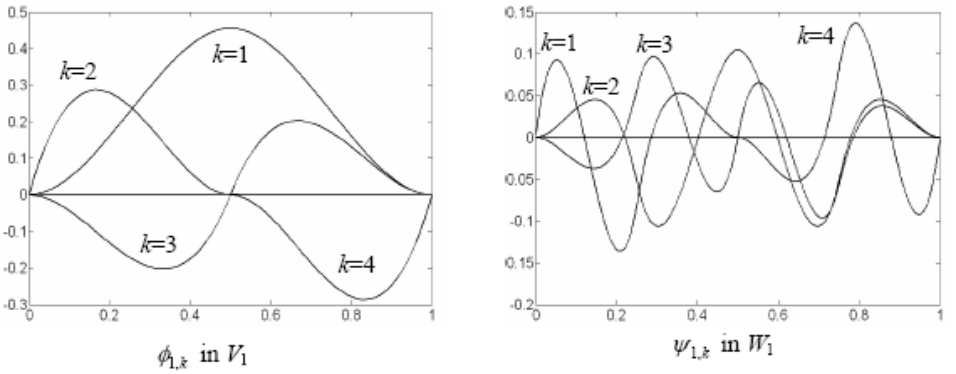

Figure 3: Scaling functions in V_1 and wavelets in W_1

The wavelet bases in V_j can be written as

$$\mathbf{\Phi}_j = [\ \mathbf{\Phi}_1 \quad \boldsymbol{\psi}_1 \quad \boldsymbol{\psi}_2 \quad \cdots \quad \boldsymbol{\psi}_{j-1}] \tag{7}$$

where $\mathbf{\Phi}_1 = [\phi_{1,1}, \phi_{1,2}, \phi_{1,3}, \phi_{1,4}]$ denotes scaling functions in V_1 and $\boldsymbol{\psi}_s (s = 1,2,\ldots,j-1$) consists of the wavelet base in W_s, i.e. $\boldsymbol{\psi}_s = [\psi_{s,1}, \psi_{s,2}, \ldots, \psi_{s,2^{s+1}}]$.

2.2 Multi-scale wavelet-based beam element

At a certain scale j,the wavelet-based Rayleigh-Timoshenko beam element considering the effects of the cross-section inertia and shear deformation was constructed in Ref. (Xiang, et al., 2007), the corresponding elemental free vibration frequency equation is

$$|\mathbf{K}^e - \omega^2 \mathbf{M}^e| = 0, \tag{8}$$

where ω is the natural angular frequency(rad/s), $\mathbf{K}^e$ is the elemental stiffness matrix, and $\mathbf{M}^e$ is the elemental mass matrix (Xiang, et al., 2007). To obtain stifness and mass matrices, we have to compute the integration as follows

$$\begin{cases} \mathbf{\Gamma}_j^{1,1} = \int_0^1 \frac{d\mathbf{\Phi}_j^{\mathrm{T}}}{d\xi} \frac{d\mathbf{\Phi}_j}{d\xi} d\xi \\ \mathbf{\Gamma}_j^{1,0} = \int_0^1 \frac{d\mathbf{\Phi}_j^{\mathrm{T}}}{d\xi} \mathbf{\Phi}_j d\xi \\ \mathbf{\Gamma}_j^{0,0} = \int_0^1 \mathbf{\Phi}_j^{\mathrm{T}} \mathbf{\Phi}_j d\xi \end{cases} \tag{9}$$

We start with an initial coarse approximation space V_1 and the scaling functions $\mathbf{\Phi}_1$ are used. Then the wavelet bases are inductively added. We can use the multi-resolution properties of the wavelet bases of Hermite cubic splines on the interval, i.e.,

$$V_j = V_1 \dot{+} W_1 \dot{+} W_2 \dot{+} \cdots \dot{+} W_{j-1}, \tag{10}$$

where $\dot{+}$ denotes direct sum.

It should be pointed out that the wavelets spaces by themselves form a complete space. Therefore, the unknown function could be expanded entirely in terms of the wavelets. However, to retain only a finite number of terms in the expansion, the scaling function space V_1 must be included.

The key to the multi-scale solution of shafts is to compute the integral as show in Eq.(9). For integral $\mathbf{\Gamma}_j^{1,1} = \int_0^1 \frac{d\mathbf{\Phi}_j^{\mathrm{T}}}{d\xi} \frac{d\mathbf{\Phi}_j}{d\xi} d\xi$,the multi-scale matrix is

$$\mathbf{\Gamma}_j^{1,1} = \begin{bmatrix} \mathbf{A}_{\mathbf{\Phi}_1,\mathbf{\Phi}_1} & \mathbf{A}_{\mathbf{\Phi}_1,\boldsymbol{\psi}_1} & \cdots & \mathbf{A}_{\mathbf{\Phi}_1,\boldsymbol{\psi}_{j-1}} \\ & \mathbf{A}_{\boldsymbol{\psi}_1,\boldsymbol{\psi}_1} & \cdots & \mathbf{A}_{\boldsymbol{\psi}_1,\boldsymbol{\psi}_{j-1}} \\ sym- & & \ddots & \vdots \\ & & & \mathbf{A}_{\boldsymbol{\psi}_{j-1},\boldsymbol{\psi}_{j-1}} \end{bmatrix} \tag{11}$$

where the sub-matrix of $\mathbf{\Gamma}_j^{1,1}$ can be calculated by $\mathbf{A}_{\mathbf{x},\mathbf{y}} = \int_0^1 \frac{d\mathbf{x}^{\mathrm{T}}}{d\xi} \frac{d\mathbf{y}^{\mathrm{T}}}{d\xi} d\xi, (\mathbf{x},\mathbf{y} = \mathbf{\Phi}_1, \boldsymbol{\psi}_1, \boldsymbol{\psi}_{j-1})$.

Considering the character of HCSWI, i.e. $< u', v'_n >= 0$ for all n and $< v'_m, v'_n >= 0$ for $m \neq n$, the non-diagonal sub-matrices of Eq.(11) become zeros. Thus, $\mathbf{\Gamma}_j^{1,1}$ reduces to

$$\mathbf{\Gamma}_j^{1,1} = \begin{bmatrix} \mathbf{A}_{\boldsymbol{\phi}_1,\boldsymbol{\phi}_1} & & & \\ & \mathbf{A}_{\boldsymbol{\psi}_1,\boldsymbol{\psi}_1} & & \\ & & \ddots & \\ & & & \mathbf{A}_{\boldsymbol{\psi}_{j-1},\boldsymbol{\psi}_{j-1}} \end{bmatrix} \tag{12}$$

From Eq.(12), only the diagonal sub-matrices will be calculated when we lift scale 1 to $j-1$ and other sub-matrices will remain zeros. This leads to substantial relief of computational burden.

For integral $\mathbf{\Gamma}_j^{1,0} = \int_0^1 \frac{d\mathbf{\Phi}_j^{\mathrm{T}}}{d\xi} \mathbf{\Phi}_j d\xi$, the multi-scale matrix is

$$\mathbf{\Gamma}_j^{1,0} = \begin{bmatrix} \mathbf{B}_{\mathbf{\Phi}_1,\mathbf{\Phi}_1} & \mathbf{B}_{\mathbf{\Phi}_1,\boldsymbol{\psi}_1} & \cdots & \mathbf{B}_{\mathbf{\Phi}_1,\boldsymbol{\psi}_{j-1}} \\ & \mathbf{B}_{\boldsymbol{\psi}_1,\boldsymbol{\psi}_1} & \cdots & \mathbf{B}_{\boldsymbol{\psi}_1,\boldsymbol{\psi}_{j-1}} \\ sym- & & \ddots & \vdots \\ & & & \mathbf{B}_{\boldsymbol{\psi}_{j-1},\boldsymbol{\psi}_{j-1}} \end{bmatrix} \tag{13}$$

where $\mathbf{B}_{\mathbf{x},\mathbf{y}} = \int_0^1 \frac{d\mathbf{x}^{\mathrm{T}}}{d\xi} \mathbf{y} d\xi, (\mathbf{x}, \mathbf{y} = \mathbf{\Phi}_1, \boldsymbol{\psi}_1, \boldsymbol{\psi}_{j-1})$.

For integral $\mathbf{\Gamma}_j^{0,0} = \int_0^1 \mathbf{\Phi}_j^{\mathrm{T}} \mathbf{\Phi}_j d\xi$,the multi-scale matrix is

$$\mathbf{\Gamma}_j^{0,0} = \begin{bmatrix} \mathbf{C}_{\mathbf{\Phi}_1,\mathbf{\Phi}_1} & \mathbf{C}_{\mathbf{\Phi}_1,\boldsymbol{\psi}_1} & \cdots & \mathbf{C}_{\mathbf{\Phi}_1,\boldsymbol{\psi}_{j-1}} \\ & \mathbf{C}_{\boldsymbol{\psi}_1,\boldsymbol{\psi}_1} & \cdots & \mathbf{C}_{\boldsymbol{\psi}_1,\boldsymbol{\psi}_{j-1}} \\ sym- & & \ddots & \vdots \\ & & & \mathbf{C}_{\boldsymbol{\psi}_{j-1},\boldsymbol{\psi}_{j-1}} \end{bmatrix} \tag{14}$$

where $\mathbf{C}_{\mathbf{x},\mathbf{y}} = \int_0^1 \mathbf{x}^{\mathrm{T}} \mathbf{y} d\xi, (\mathbf{x}, \mathbf{y} = \mathbf{\Phi}_1, \boldsymbol{\psi}_1, \boldsymbol{\psi}_{j-1})$.

From Eqs.(13)and (14), only sub-matrices $\mathbf{B}_{\mathbf{x},\mathbf{y}}, (\mathbf{x} = \mathbf{\Phi}_1, \boldsymbol{\psi}_1, \ldots, \boldsymbol{\psi}_l; \mathbf{y} = \boldsymbol{\psi}_l)$ and $\mathbf{C}_{\mathbf{x},\mathbf{y}}, (\mathbf{x} = \mathbf{\Phi}_1, \boldsymbol{\psi}_1, \ldots, \boldsymbol{\psi}_l; \mathbf{y} = \boldsymbol{\psi}_l)$ will be calculated when lifting scale l to $l+1$ and other sub-matrices will be preserved. This can also increase the calculating efficiency. Because multi-scale elements are successfully constructed, it can be directly incorporated into the traditional adaptive finite element framework in the analysis of forward problem for more accurate results.

2.3 Adaptive wavelet finite element scheme

The adaptive scheme is shown in Fig.4. It is important to point out that the element can be employed as an useful tool to achieve the adaptive wavelet finite element

analysis for the same problems in other research areas.

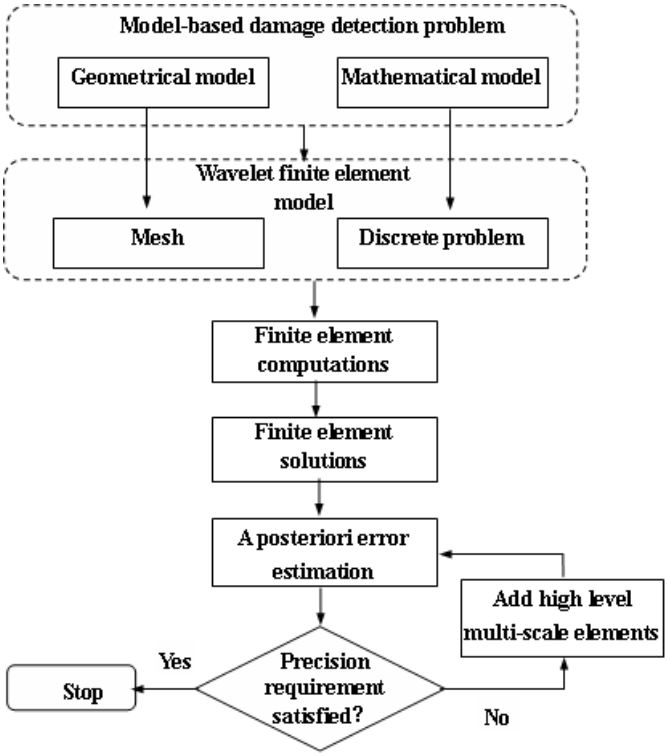

Figure 4: The diagram of adaptive wavelet finite element scheme

The effective multi-scale elements should performance well because only the high level multi-scale elements are added in some local areas with high approximation errors. Because of the fully and particular scale-decoupling characters of the present multi-scale wavelet-based elements, only the finite element equations of local areas are computed at the next iteration step, and the approximation errors are rapidly decreased after several iteration steps.

3 Multiple cracks detection

3.1 The procedure

For detecting damages, the model-based method is generally concerned with the forward problem analysis using finite element method and the inverse problem analysis using many optimization methods. These detection schemes are based

on the fact that the presence of a damage changes the dynamic characteristics of the structures.

Fig.5 shows a beam or shaft with some damages on its surface. $\beta_i = e_i/L, (i = 1, 2, \cdots, n)$ denotes the normalized location of damage i in beam, and L is the beam length.

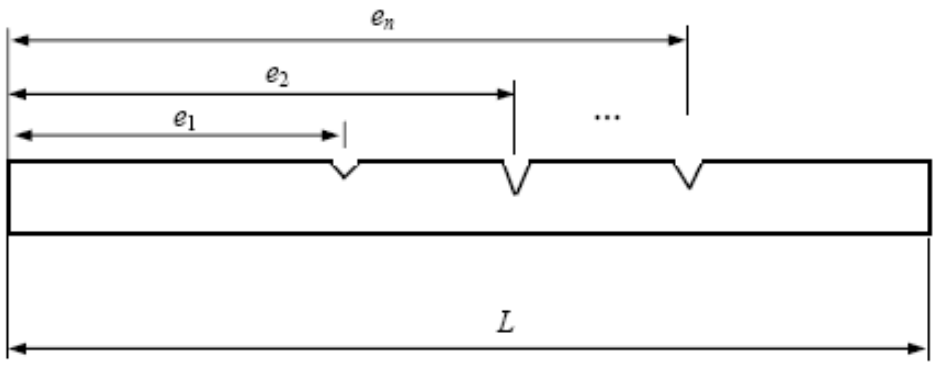

Figure 5: A beam with n damages on its surface

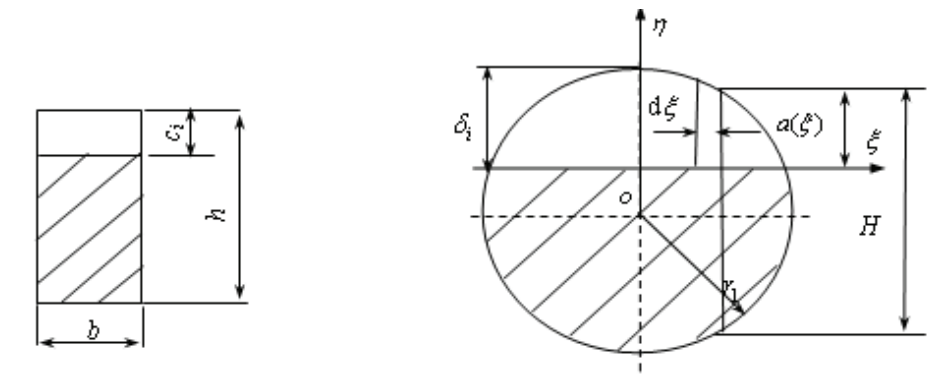

Figure 6: Damaged rectangular and circular beam cross-sections

The continuity conditions at damage position indicate that the left node j and right node $j+1$ have the same transverse displacement, namely,$u_j = u_{j+1}$, while their rotations θ_j and θ_{j+1} are connected through the damaged stiffness submatrix $\mathbf{K}_S$ as follows

$$\mathbf{K}_S = \begin{bmatrix} K_t & -K_t \\ -K_t & K_t \end{bmatrix} \tag{15}$$

The damaged cross-sections in beam with rectangle and circular cross-sections are shown in Fig.6(a) and Fig.6(b) respectively.

For a damaged beam with rectanglar section, K_t is well known in literature and is defined by (Patil and Maiti, 2003)

$$K_t = bh^2E/(72\pi\alpha_i^2 f(\alpha_i)) \tag{16}$$

in which (Tada, et al., 2000)

$$f(\alpha_i) = 0.6384 - 1.035\alpha_i + 3.7201\alpha_i^2 - 5.1773\alpha_i^3 + 7.553\alpha_i^4 - 7.332\alpha_i^5 + 2.4909\alpha_i^6 \tag{17}$$

where $\alpha_i = c_i/h$ denotes normalized damage depth as shown in Fig.6(a), E is Young's modulus, b is the beam width, h is the beam height.

For a damaged shaft, K_t is calculated by considering a damaged shaft as a combination of a series of thin strip as (Chasalevris and Papadopoulos, 2006)

$$K_t = \frac{\pi E {r_1}^8}{32(1-\mu)} \frac{1}{\int_{-r_1\sqrt{1-(1-2\alpha_i)^2}}^{r_1\sqrt{1-(1-2\alpha_i)^2}} [\int_0^{a(\xi)} \eta F^2(\eta/H) d\eta] d\xi} \tag{18}$$

where δ_i is damage depth, r_1 is radius of the shaft, μ is the Poisson's ratio, $\alpha_i = \delta_i/2r_1$ denotes normalized damage depth, $a(\xi) = 2r_1\alpha_i - (r_1 - \sqrt{r_1^2 - \xi^2})$ is the damage depth of a thin strip, $H = 2\sqrt{r_1^2 - \xi^2}$ is the height of thin strip $F(\eta/H)$ is stress intensity function which is given by the following experimental formula (Tada, et al., 2000)

$$F(\eta/H) = 1.122 - 1.40(\eta/H) + 7.33(\eta/H)^2 - 13.08(\eta/H)^3 + 14.0(\eta/H)^4 \tag{19}$$

According to the normalized damage location $\beta_i = e_i/L, (i = 1, 2, \cdots, n)$, we can assemble damaged stiffness submatrix into the global multi-scale wavelet-based elemental stiffness matrix in the corresponding place. The procedure is similar to that for single damage detection using wavelet finite element method (Xiang,

et al., 2007). The global mass matrix of damaged structure is the same as the undamaged one. Then the damaged structural finite element model of wavelet-based elements can be constructed. The solution of the eigenvalue problem can then proceed as usual. Therefore, the free vibration frequency equation for multi degree of freedoms (MDOFs) system is

$$\left| \ \bar{\mathbf{K}} - \omega^2 \bar{\mathbf{M}} \ \right| = 0 \tag{20}$$

where $\bar{\mathbf{K}}$ and $\bar{\mathbf{M}}$ are the global stiffness and mass matrices.

To construct an accurate damage detection database, the multi-scale wavelet-based element proposed herein is applied to the forward problem analysis. The functions of the lowest frequencies of damage locations and depths are obtained as follows

$$\omega_j = F_j(\alpha_1, \alpha_2, \cdots, \alpha_n, \beta_1, \beta_2, \cdots, \beta_n), (j = 1, 2, 3, \cdots, 2n) \tag{21}$$

where n is the number of damages in a beam.

3.2 Solving the inverse problem

To detect n damages in a structure, inverse problem analysis is necessary step, which considers the measurement of several lowest frequencies and searches for locations and depths of the damaged structures from damage detection databases by forward problem analysis. From the groundbreaking studies presented by Dilena and Morassi (Dilena and Morassi,2009; 2010; Morassi, 2007; Gaddemi and Morassi, 2007), if there exist n damages, $2n$ frequencies are the least inputs to detect these damages. Therefore, the first $2n$ frequencies should be measured to seek for optimum damage parameters. Based on Eq.(21), we have

$$(\alpha_1, \alpha_2, \cdots, \alpha_n, \beta_1, \beta_2, \cdots, \beta_n) = F_j^{-1}(\omega_j), (j = 1, 2, 3, \cdots, 2n) \tag{22}$$

From Eq.(22),we can see clearly that the inverse problem of multiple damages detection is in essential a discrete optimization problem from damage detection database computed by multi-scale wavelet-based beam elements.

To evaluate the errors of the inputs frequencies obtained by experimental measurement of real structures, Euclidean length (EL) is adopted in this study as

$$EL = \sqrt{(\omega_1 - \breve{\omega}_1)^2 + (\omega_2 - \breve{\omega}_2)^2 + \ldots + (\omega_{2n} - \breve{\omega}_{2n})^2} \tag{23}$$

where ω_1, ω_2, …, ω_{2n} are the $2n$ frequencies in the damage detection database, whereas $\breve{\omega}_1$, $\breve{\omega}_2$, …, $\breve{\omega}_{2n}$ denote the measured frequencies by experimental modal analysis (EMA) or operational modal analysis (OMA).

The commonly used root-mean-square (RMS) value obtained from Euclidean length is defined by

$$RMS = EL/\sqrt{2n} \tag{24}$$

where $2n$ is the number of input frequencies.

The procedure for multiple damage detection is presented in Fig.7

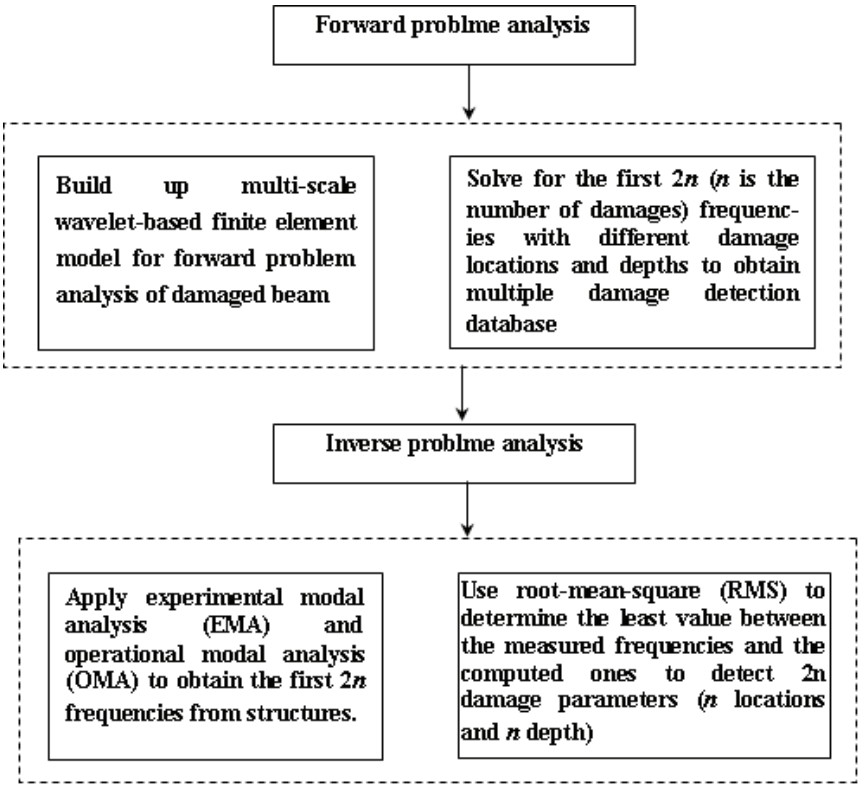

Figure 7: The multiple damage detection procedure

4 Numerical simulation

To examine the performance of the proposed method, two examples are given herein. One is a beam of rectangle cross-section with two damages on its surface and the other is a beam of circular cross-section (or shaft) with two damages .

Example 1 Consider a damaged steel cantilever beam. Its dimensions are: $L \times h \times b = 0.85m \times 0.02m \times 0.012m$. Material parameters are: Young's modulus $E = 2.06 \times 10^{11} N/m^2$,Poisson's ratio $\mu = 0.3$ and density $\rho = 7860 kg/m^3$.

Multi-scale wavelet-based beam element using HCSWI bases at level $j = 2$ are used, and the size of the multi-scale wavelet-based beam element is 32×32 (32 DOFs).In this study, three multi-scale wavelet-based beam elements are used. For comparison, the traditional Timoshenko beam elements with size 768×768(768DOFs) are used as benchmark. The results computed at level $j = 2$ are found to be in good agreement with those computed by the Timoshenko beam elements with 768DOFs , as shown in Table 1. To obtain a same precision, using wavelet-based elements, only 1/24 of the DOFs of traditional Timoshenko beam elements are needed. The good performance of the lifting scheme is observed when the wavelets are added step by step to generate multi-scale wavelet-based elements.

From Table 1, It is also expected that the natural eigenfrequency of a damaged beam are lower than those of the undamage one. This is due to the reduction of beam stiffness caused by the damages. Also, since the natural frequency is a function of stiffness, a deeper damage causes greater reduction in natural frequency. Moreover, there are four damage parameters that describe clearly the existence of two damages in a beam, i.e., the two damage location β_1 and β_2 as well as the two damage depth α_1 and α_2. The first case in Table 1 shows the first four frequencies of undamage beam (this is often employed as a benchmark to update numerical model) and the second case shows the first four frequencies of only one damage exist in a beam (This is the special case that one damage location equals to another) with the damage parameters $\beta_1 = \beta_2 = 0.3$ and $\alpha_1 = \alpha_2 = 0.2$.

In the following, the way each of these four damage parameters affect the vibration will be investigated. When two damage parameters retain ceratin values, five-dimension damage detection database is reduced to three-dimension. Therefore, to make a clearly description, it is supposed that the two parameters of damages locations and depths are constant in the present study. It should be pointed out that the same procedure can obviously be repeated for all the locations and depths.

Fig.8 shows results of the first four frequencies as functions of single damage in a beam, i.e., damage detection parameters are: $\alpha_1 = \alpha_2 = \alpha$ and $\beta_1 = \beta_2 = \beta$. As shown in Fig.8, the change of the first four frequencies due to the influence of damage location and depth are similar to that in (Xiang, et al., 2007).

Fig.8(a), (b), (c), (d) show the first, second, third and fourth frequencies respectively. Some results are explained as follows:

(1) Effects of damage location β: It can be seen that the change in the first four natural frequencies are affected when the damage is located at every damage location.

Table 1: Comparison of the frequencies results obtained by the present element and those by traditional Timoshenko beam elements

Case				Wavelet-based elements				Traditional Timoshenko elements			
α_2	α_1	β_2	β_1	ω_1	ω_2	ω_3	ω_4	ω_1	ω_2	ω_3	ω_4
0	0	0	0	143.84	901.42	2524.00	4946.05	143.82	901.38	2524.16	4946.23
0.2	0.2	0.3	0.3	142.87	899.70	2503.64	4933.89	142.83	899.72	2503.69	4933.92
0.2	0.2	0.3	0.1	140.87	894.97	2501.05	4933.64	140.85	895.02	2501.11	4933.71
0.2	0.3	0.3	0.1	138.34	889.17	2497.91	4933.37	138.36	889.11	2497.84	4933.42
0.2	0.4	0.3	0.1	134.49	880.77	2493.42	4932.99	134.52	880.82	2493.53	4933.11
0.2	0.3	0.4	0.2	139.97	895.20	2497.06	4848.37	139.88	895.31	2496.95	4848.73
0.3	0.3	0.4	0.2	139.25	887.47	2484.61	4832.92	139.19	887.55	2484.73	4832.80
0.4	0.3	0.4	0.2	138.09	875.57	2465.93	4809.67	138.04	875.62	2465.87	4809.79
0.2	0.5	0.5	0.3	136.48	881.04	2386.86	4805.35	136.39	881.18	2386.97	4805.61
0.3	0.5	0.5	0.3	136.11	870.84	2386.10	4743.85	136.07	870.78	2386.21	4743.72
0.4	0.5	0.5	0.3	135.51	855.13	2384.92	4654.23	135.61	855.22	2385.07	4654.33
0.4	0.4	0.6	0.4	140.60	845.27	2418.74	4872.25	140.57	845.18	2418.65	4872.33
0.5	0.4	0.6	0.4	140.14	824.66	2381.59	4852.11	140.17	824.73	2381.65	4852.22
0.6	0.4	0.6	0.4	139.49	797.93	2337.47	4827.76	139.51	797.97	2337.49	4827.84
0.1	0.3	0.7	0.5	143.08	880.31	2516.81	4837.57	143.12	880.35	2516.78	4837.62
0.1	0.2	0.7	0.5	143.50	891.44	2516.83	4895.11	143.48	891.37	2516.78	4895.29
0.1	0.4	0.7	0.5	142.39	863.26	2516.79	4753.68	142.36	863.32	2516.71	4753.59

For a certain damage depth,the first frequency would be decreased significantly with respect to the larger damage location. Moreover, it also shown that the second, third and fourth natural frequencies are almost unaffected for some damage locations. The reason is that the nodal points for these functions are located at those position.

(2) Effects of damage depth α: It is noticed that the change in the first four natural frequencies are affected when the single damage is occurred at every depth. For a certain damage location, three frequencies would monotonically decrease if the larger damage size is given. From the above observations, it could be stated that the change in frequencies is not only a function of the damage location but also that of the damage depth.

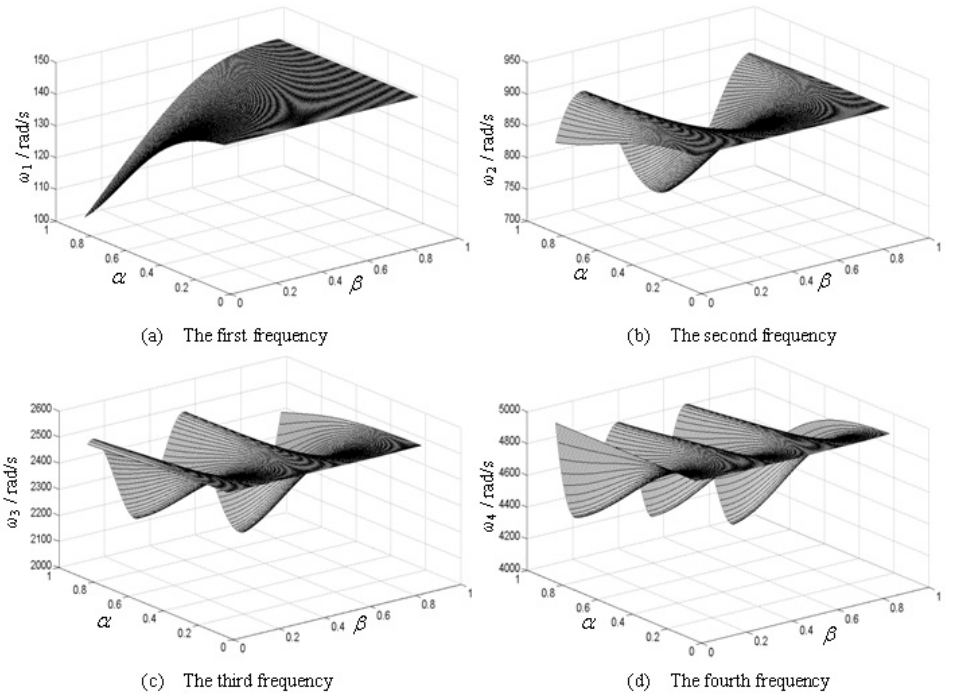

Figure 8: The first four frequencies as functions of only one damage occurred in a beam

Fig.9 shows the first four frequencies as functions of the second damage's α_2 and β_2 with α_1 and β_1 fixed at 0.3 and 0.1 respectively. When one damage is kept constant($\alpha_1 = 0.3$ and $\beta_1 = 0.1$), the relationships between the first four frequencies and α_2 and β_2 are shown in Fig.9(a), (b), (c) and (d) respectively. It is observed that

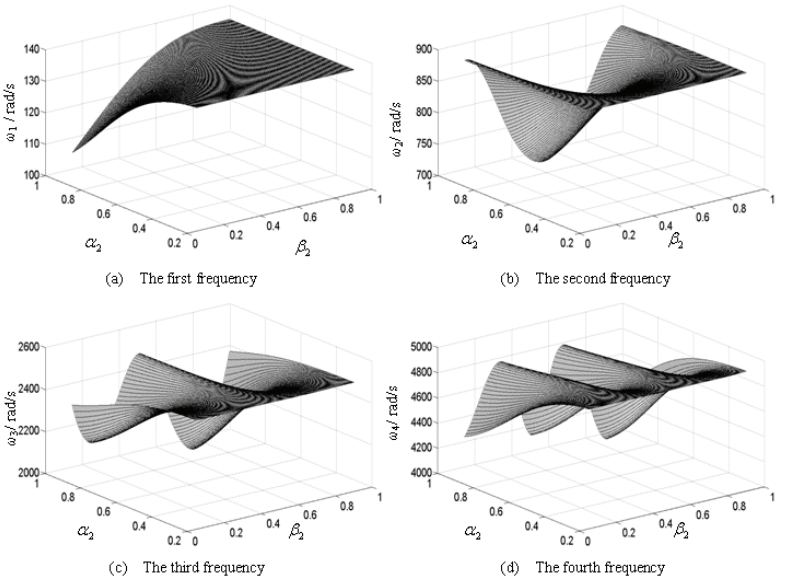

Figure 9: The first four frequencies as functions of the second damage's α_2 and β_2 with $\alpha_1 = 0.3$ and $\beta_1 = 0.1$

the diagrams are similar to those in Fig.8. However, the first four frequencies are decreased substantially compared with only the single damage case. Therefore, we can easily distinguish the existence of one or two damages by the proposed method.

The first four frequencies as functions of α_2 and α_1 when β_2 and β_1 are fixed at 0.5 and 0.3 respectively shown in Fig.10 to examine the effect of damage depth on the first four frequencies. From Fig.10(a),(b),(c) and (d), it is shown that the damages' depth has a strong impact on the frequencies. The first frequency varies from nearly 140 rad/s to 110 rad/s, far from the undamage frequency (143.84 rad/s) as shown in Table 1. The second, third and fourth frequencies vary from approximately 880 rad/s to 700 rad/s, 2500 rad/s to 2100 rad/s and 4800 rad/s to 4000 rad/s, respectively, which are also far below the undamage frequency (901.42 rad/s, 2524.00 rad/s and 4946.05 rad/s, respectively) as shown in Table 1. It is also observed that larger damage depths lead to larger decrease in natural frequencies.

To explore the effect of the damage location on natural frequency change, we plot some results in Fig. 11. It shows that the first four frequencies as functions of the damages locations β_2 and β_1 with $\alpha_2 = 0.3$ and $\alpha_1 = 0.4$. From Fig.11 (a), (b), (c),

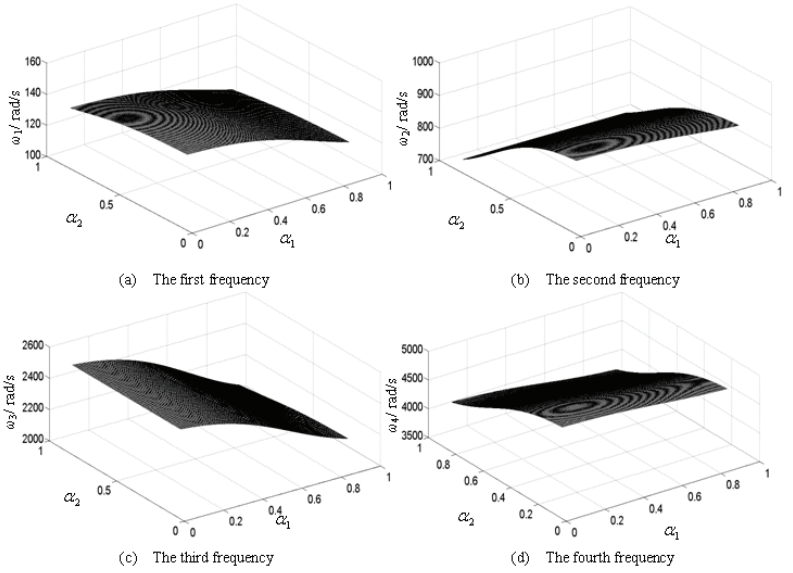

Figure 10: The first four frequencies as functions of the damages' α_2 and α_1 with the damages' $\beta_2 = 0.5$ and $\beta_1 = 0.3$

(d) and compared with Fig.10, it can be seen clearly that the damage locations have less impact on the natural frequencies comparing to the damage depths. There also exist minimum frequencies when the damage locations β_1 and β_2 become larger, i.e., when the damage locations moved to the free end of clamped beam.

In the simulation of the present method, the measured first four frequencies for the damage detection are replaced by the first four simulation frequencies computed by traditional Timshenko beam element as shown in Table 1. The comparison of predicted and actual damage locations and depths is shown in Table 2. The predicted damage locations and depths are 100 % accurate. It should be pointed out that if there exist measured errors introduced by measuring systems, structural boundary conditions, material inner damping, etc., the prediction will not be 100 % accurate (Chasalevis and Papadopoulos, 2006). However, we can select the agreeable minimum root-mean-square (RMS) values to determine the damage parameters. The results in Table 2 can also help to determine the actual number of damages. For example in case 2, $\beta_1 = \beta_2 = 0.3$ indicates that there is only one damage; for case 1, $\alpha_1 = \alpha_2 = 0$ implies no damage. In general, the number of damages is equal to

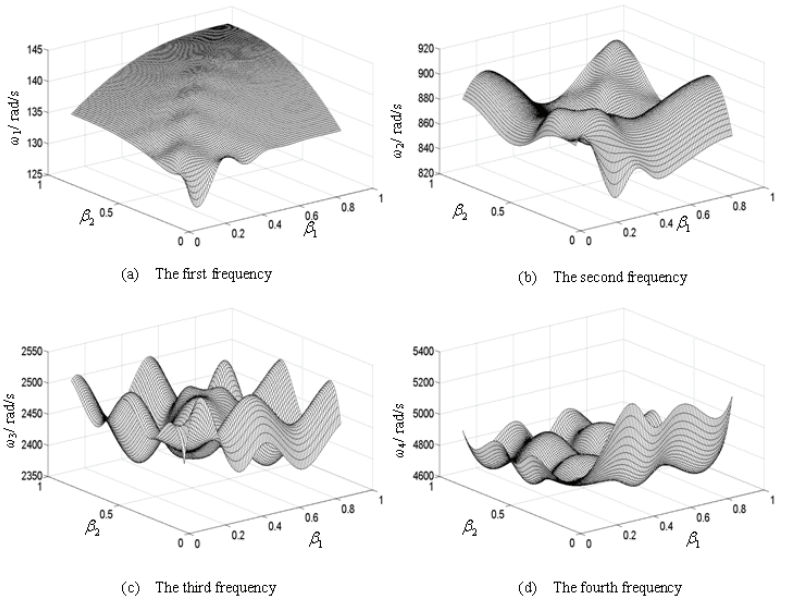

Figure 11: The first four frequencies as functions of the damages' β_2 and β_1 with the damages' $\alpha_2 = 0.3$ and $\alpha_1 = 0.4$

the number of different beta values each associate to a non-zero alpha.

Example 2 Consider a simply supported shaft of $0.85m$ long. The Young's modulus $E = 2.06 \times 10^{11} N/m^2$, the cross-section radius $d = 0.02m$, Poisson's ratio $\mu = 0.3$ and the material density $\rho = 7860 kg/m^3$.

Multi-scale wavelet-based HCSWI beam elements at level $j = 2$ are used, and only 32 DOFs are needed. The traditional Timoshenko beam elements with 768DOFs are also used for comparison. The two results are quite agreeable, as shown in Table 3, although the number of DOFs needed for the wavelet-based elements is only 1/24 of that for the Timoshenko elements.

For the cases investigated, the first four frequencies as functions of α_2 and β_2 with $\alpha_1 = 0.3$ and $\beta_1 = 0.1$ can be seen in Fig.12(a),(b),(c),(d). It is observed that the diagrams are similar to those in Fig.9 for a rectangle cross-section beam. Moreover, the change of natural frequencies for the simply supported shaft with two damages are much more pronounced.

For the simulation purpose, the first four measured frequencies for the damage de-

Table 2: Detection results and RMS values for a clamped beam

Case	Input frequencies				Detected parameters				RMS
	ω_1	ω_2	ω_3	ω_4	α_2	α_1	β_2	β_1	
1	143.82	901.38	2524.16	4946.23	0	0	0	0	0.12
2	142.83	899.72	2503.69	4933.92	0.2	0.2	0.3	0.3	0.04
3	140.85	895.02	2501.11	4933.71	0.2	0.2	0.3	0.1	0.05
4	138.36	889.11	2497.84	4933.42	0.2	0.3	0.3	0.1	0.05
5	134.52	880.82	2493.53	4933.11	0.2	0.4	0.3	0.1	0.09
6	139.88	895.31	2496.95	4848.73	0.2	0.3	0.4	0.2	0.20
7	139.19	887.55	2484.73	4832.80	0.3	0.3	0.4	0.2	0.10
8	138.04	875.62	2465.87	4809.79	0.4	0.3	0.4	0.2	0.08
9	136.39	881.18	2386.97	4805.61	0.2	0.5	0.5	0.3	0.16
10	136.07	870.78	2386.21	4743.72	0.3	0.5	0.5	0.3	0.09
11	135.61	855.22	2385.07	4654.33	0.4	0.5	0.5	0.3	0.11
12	140.57	845.18	2418.65	4872.33	0.4	0.4	0.6	0.4	0.08
13	140.17	824.73	2381.65	4852.22	0.5	0.4	0.6	0.4	0.07
14	139.51	797.97	2337.49	4827.84	0.6	0.4	0.6	0.4	0.05
15	143.12	880.35	2516.78	4837.62	0.1	0.3	0.7	0.5	0.04
16	143.48	891.37	2516.78	4895.29	0.1	0.2	0.7	0.5	0.10
17	142.36	863.32	2516.71	4753.59	0.1	0.4	0.7	0.5	0.07

tection are also replaced by the first four simulation frequencies computed using traditional Timshenko beam element as shown in Table 3. The comparison of predicted and actual damage locations and depths is shown in Table 4.The predicted damage locations and depths are again 100 %. Once again, we can identify the number of damages based on the alpha and beta values that are determined by the minimum RMS shown in Table 4.

The above two examples clearly demonstrate that the proposed method yield results comparable to these of the Timoshenko method with substantially fewer number of elements. The computational time for the forward problem can thus be reduced considerably. The inverse problem can also be solved to determine the number of damages, their locations and severity based on the minimum RMS values.

5 Experimental investigation

In this section, a laboratory experiment on a test beam structure is conducted to demonstrate and verify the proposed multiple damage detection method.

Table 3: Comparison of frequencies obtained using the proposed elements and the Timoshenko beam elements

Case				Wavelet-based elements				Traditional Timoshenko elements			
α_2	α_1	β_2	β_1	ω_1	ω_2	ω_3	ω_4	ω_1	ω_2	ω_3	ω_4
0	0	0	0	349.66	1398.69	3147.28	5596.33	349.67	1398.67	3147.00	5596.12
0.2	0.2	0.3	0.3	348.26	1391.04	3145.97	5588.08	348.12	1390.87	3145.38	5588.25
0.2	0.2	0.3	0.1	348.26	1391.04	3145.97	5588.08	348.21	1390.96	3146.10	5588.23
0.2	0.3	0.3	0.1	348.06	1388.14	3133.46	5556.36	348.11	1388.23	3133.37	5556.52
0.2	0.4	0.3	0.1	347.72	1383.37	3113.06	5505.92	347.69	1383.45	3113.15	5506.10
0.2	0.3	0.4	0.2	347.12	1374.88	3077.38	5421.63	347.07	1374.97	3077.29	5421.88
0.3	0.3	0.4	0.2	345.79	1375.91	3096.14	5537.15	345.83	1375.85	3096.01	5537.34
0.4	0.3	0.4	0.2	342.71	1371.77	3084.35	5490.07	342.67	1371.66	3084.51	5489.93
0.2	0.5	0.5	0.3	337.39	1364.76	3064.50	5414.98	337.43	1364.81	3064.32	5415.12
0.3	0.5	0.5	0.3	335.70	1337.64	3113.05	5500.86	335.65	1337.73	3113.16	5501.09
0.4	0.5	0.5	0.3	332.59	1337.53	3081.77	5500.68	332.64	1337.46	3081.93	5500.32
0.4	0.4	0.6	0.4	329.64	1366.09	3082.15	5280.53	329.59	1366.17	3082.33	5280.25
0.5	0.4	0.6	0.4	324.33	1357.05	3066.17	5203.13	324.38	1357.09	3066.26	5202.95
0.6	0.4	0.6	0.4	305.69	1327.53	3014.17	4986.86	305.73	1327.42	3014.02	4987.04
0.1	0.3	0.7	0.5	343.81	1397.15	3097.72	5593.22	343.78	1397.24	3097.96	5593.46
0.1	0.2	0.7	0.5	347.25	1397.15	3127.70	5593.22	347.22	1397.06	3127.88	5593.51
0.1	0.4	0.7	0.5	337.91	1397.15	3048.44	5593.22	337.88	1397.22	3048.18	5593.08

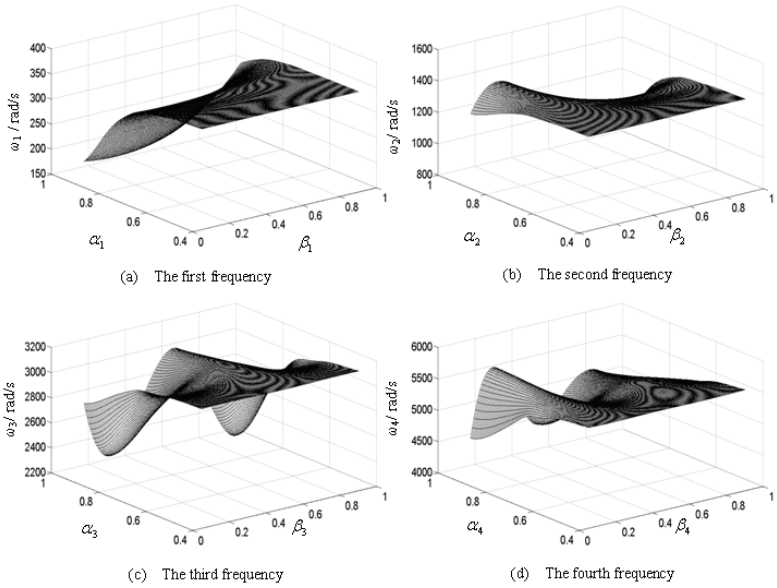

Figure 12: The first four frequencies as functions of the second damage's α_2 and β_2 with the first damage $\alpha_1 = 0.3$ and $\beta_1 = 0.1$

5.1 Experimental setup and description

Fig.13 shows a schematic overview of the setup. The test system consists of a cantilever beam with two damages, a tiny accelerometer, an impact hammer, a signal conditioner, data acquisition card and a computer with Fast Fourier Transform (FFT) program. The geometry of the cantilever beam is shown in Fig.14. Its dimensions are: $L \times h \times b = 0.5m \times 0.019m \times 0.012m$. The cantilever material is structural steel with Young's modulus $E = 2.06 \times 10^{11} N/m^2$, Possion's ratio $\mu = 0.3$ and density $\rho = 7860 kg/m^3$.

We tested one intact and three damaged beams as shown in Fig.15. The locations and depths of the two damages are $\beta_1 = e_1/L$, $\beta_2 = e_2/L$, $\alpha_1 = c_1/h$ and $\alpha_2 = c_2/h$, respectively. The specific parameters are shown in Table 5.

In the experimental study, the sampling frequency f_s is 5,000 Hz and 10,000 data points are collected. For each case as shown in Table 5, the impulse response signal and the associated frequency spectrum are plotted in Fig.16. It can be seen clearly that the first four frequencies of cantilever beam are captured for every case.

Table 4: Detection results and RMS values for a shaft

Case	Input frequencies				Detected parameters				RMS
	ω_1	ω_2	ω_3	ω_4	α_2	α_1	β_2	β_1	
1	348.21	1390.96	3146.10	5588.23	0	0	0	0	0.18
2	348.12	1390.87	3145.38	5588.25	0.2	0.2	0.3	0.3	0.11
3	348.11	1388.23	3133.37	5556.52	0.2	0.2	0.3	0.1	0.11
4	347.69	1383.45	3113.15	5506.10	0.2	0.3	0.3	0.1	0.11
5	347.07	1374.97	3077.29	5421.88	0.2	0.4	0.3	0.1	0.14
6	345.83	1375.85	3096.01	5537.34	0.2	0.3	0.4	0.2	0.12
7	342.67	1371.66	3084.51	5489.93	0.3	0.3	0.4	0.2	0.12
8	337.43	1364.81	3064.32	5415.12	0.4	0.3	0.4	0.2	0.12
9	335.65	1337.73	3113.16	5501.09	0.2	0.5	0.5	0.3	0.14
10	332.64	1337.46	3081.93	5500.32	0.3	0.5	0.5	0.3	0.20
11	327.28	1337.45	3030.42	5500.67	0.4	0.5	0.5	0.3	0.17
12	329.59	1366.17	3082.33	5280.25	0.4	0.4	0.6	0.4	0.17
13	324.38	1357.09	3066.26	5202.95	0.5	0.4	0.6	0.4	0.11
14	305.73	1327.42	3014.02	4987.04	0.6	0.4	0.6	0.4	0.13
15	343.78	1397.24	3097.96	5593.46	0.1	0.3	0.7	0.5	0.18
16	347.22	1397.06	3127.88	5593.51	0.1	0.2	0.7	0.5	0.18
17	337.88	1397.22	3048.18	5593.08	0.1	0.4	0.7	0.5	0.15

Table 5: Data of the beams

Case	e_1/mm	c_1/mm	e_2/mm	c_2/mm	β_1	α_1	β_2	α_2
0(Intact)	N/A	N/A	N/A	N/A	N/A	N/A	N/A	N/A
1	260	6	380	3	0.52	0.32	0.76	0.16
2	260	8	380	6	0.52	0.42	0.76	0.32
3	140	4	320	6	0.28	0.21	0.64	0.32

Considering the possible variations in test environment including the fluctuations in temperature, humidity and boundary conditions, ten replications are performed for each case. The average results are summarized in Table 6.

5.2 Wavelet finite element model updating and damage detection

Multi-scale wavelet-based beam element using HCSWI bases at level j=2 are employed for the experimental cantilever beam. In most cases, however, there exist

Table 6: Metrical frequencies of damaged cantilever beam and the values of corrected E_m^i (i=1, 2, 3, 4)

Case	$f_1(Hz)$	E_m^1	$f_2(Hz)$	E_m^2	$f_3(Hz)$	E_m^3	$f_4(Hz)$	E_m^4
0	56.35	1.67×10^{11}	333.42	1.48×10^{11}	921.26	1.44×10^{11}	2152.32	1.98×10^{11}
1	55.79		322.58		910.53		2088.02	
2	55.51		312.35		865.39		2065.37	
3	55.53		326.50		857.56		2077.82	

Table 7: Two damage detection results and errors

Case	β_1	α_1	β_2	α_2	β_1^* (%)	α_1^*(%)	β_2^* (%)	α_2^* (%)	RMS
1	0.52	0.32	0.76	0.16	0.50(3.8)	0.30(6.3)	0.75(1.3)	0.15(6.3)	1.64
2	0.52	0.42	0.76	0.32	0.50(3.8)	0.40(4.8)	0.75(1.3)	0.30(6.3)	14.38
3	0.28	0.21	0.64	0.32	0.30(7.1)	0.20(4.8)	0.65(1.6)	0.30(6.3)	13.18

Note: % denotes error in %.

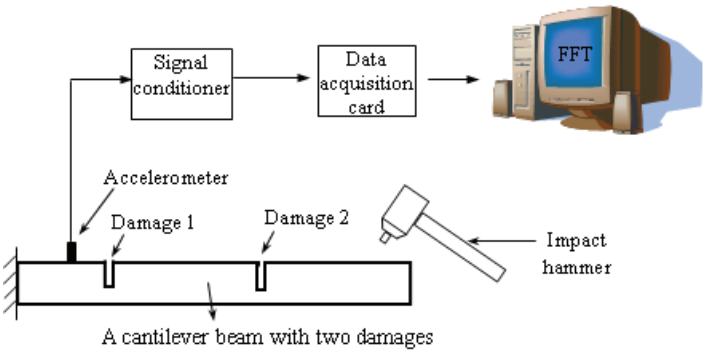

Figure 13: A schematic overview of the setup

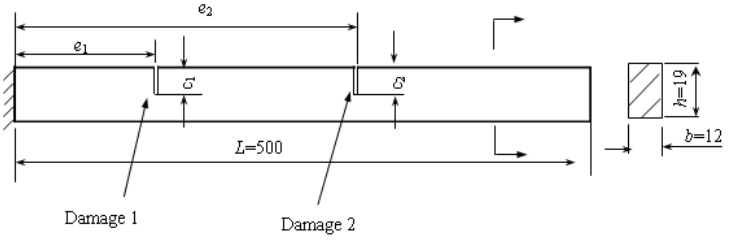

Figure 14: The geometry of cantilever beam with two damages

inevitable errors between the computational results of wavelet finite model and the metrical ones. To reduce these errors, the 'zero-setting' procedure described by Adams (Adams, et al. 1978) is used. In this procedure, the Young's modulus of the structure is modified using the natural frequencies of undamaged structure. Therefore, we have the follow iterative formula

$$|\omega_i^2 \overline{\mathbf{M}} - E_m^i \frac{\overline{\mathbf{K}}}{E}| = 0 \tag{25}$$

Figure 15: One intact and three damaged beams

where E_m^i is the i^{th} corrected value of Young's modulus E, which can be acquired through solving Eq. (25) for each frequency. It should be noted that the purpose to modify the Young's modulus is not to change the value of E but to make the metrical undamaged natural frequencies match the computed ones. This procedure can greatly reduce the error between theoretical and the experimental results, which are caused by boundary condition and material parameters. The measured frequencies of damaged cantilever beams and the values of corrected $E_m^i (i = 1,2,3,4)$ are shown in Table 6.

Table 7 shows the predicted parameters β_1^*, α_1^*, β_2^* and α_2^* of the two damages for each faulty beam. The relative errors between the predicted damage parameters and the actual damage parameters are also listed in Table 7. For the given cases, the relative errors of β_1^* and β_2^* are not more than 7.1%, whereas the relative errors of α_1^* and α_2^* are within 6.3 %. Hence, the proposed multiple damage detection method is considered to be valid for actual applications in detecting multiple damages in beams.

6 Conclusions

A new method for detecting multiple damages in beam-like structures has been proposed. This method is based on multi-scale wavelet-based beam elements with RMS of the difference between the measured and computed frequencies as the search criterion. The multi-scale wavelet-based finite element model is constructed based on the linear fracture mechanics to obtain more accurate natural frequencies of the damaged structures. The simulation and experimental results have shown that the proposed method can handle both the forward and inverse problems very well. Thus a reliable damage detection database can be obtained by solving the forward problem and the number of damages, their locations and depths can be

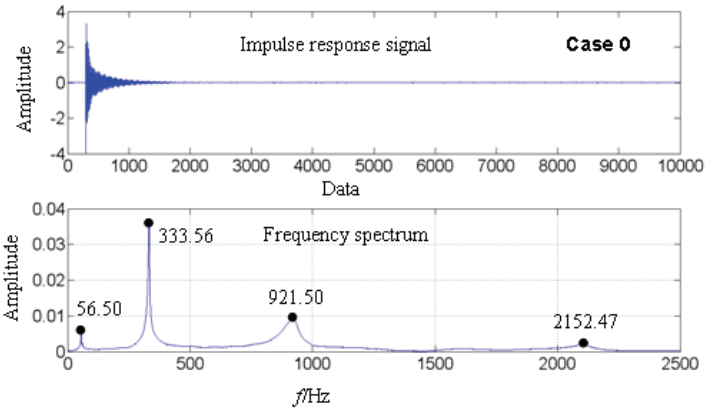

(a) case 0

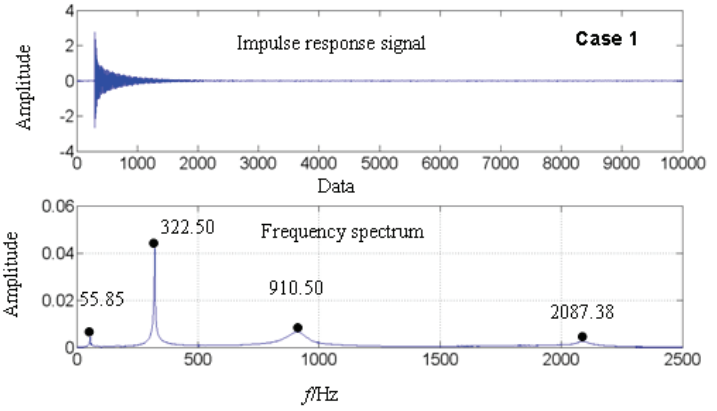

(b)case 1

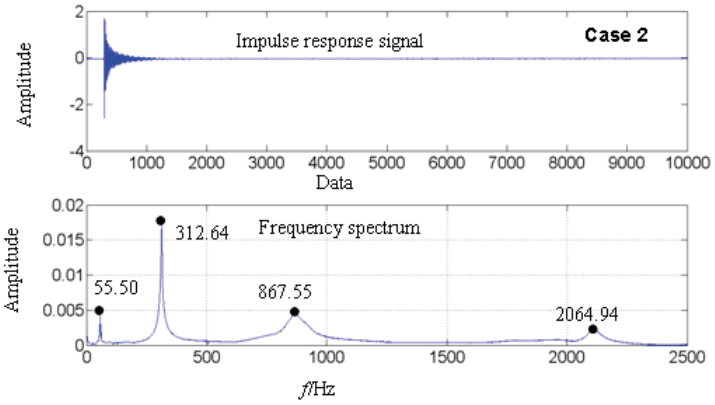

(c)case 2

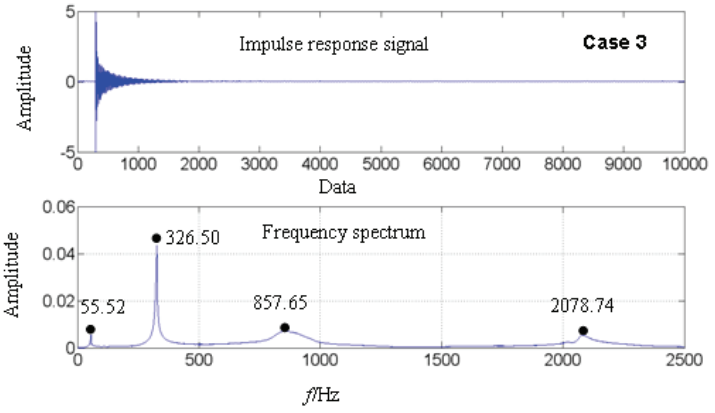

(d)case 3

Figure 16: The impulse response signal and the corresponding frequency spectrum

determined based on the inverse problem solutions.

Acknowledgement: The authors are grateful to the support from the Natural Sciences and Engineering Research Council of Canada. This work is also supported in part by the Ontario Centers of Excellence and the Excellent Talent Project of Guangxi University System, which are very much appreciated. The authors would also like to thank Mr. John Perrins of the University of Ottawa and Dr. X. Wu of the National Research Council of Canada for their technical support in machining the test beams.

References

Adams,R.D.; Cawley,P.; Pye, C.J.; Stone, B.J.(1978): A vibration technique for non-destructively assessing the integrity of structures. *Journal Mechanical Engineering Science*, vol. 20, pp. 93-100.

Caddemi, S.; Morassi, A. (2007): Damage detection and generalized Fourier coefficients. *International Journal of Solids and Structures*, vol. 44, pp. 5301-5315.

Chasalevris, A.C.; Papadopoulos,C.A.(2006): Identification of multiple cracks in beams under bending. *Mechnanical Systems and Signal Processing*, vol. 20 , pp. 1631-1673.

Chen, W.H.; Wu, C.W.(1995): A spline wavelets element method for frame structures vibration. *Computational Mechanics*, vol.16, pp.11-21.

Chen, W.H; Wu, C.W. (1996a): Extension of spline wavelets element method to membrane vibration analysis. *Computational Mechanics*, vol. 18, pp.46-54.

Chen, W.H.; Wu, C.W.(1996b): Adaptable Spline Element for Membrane Vibration Analysis. *International Journal for Numerical Methods in Engineering*, vol. 39,pp. 2457-2476.

Chen, X.F.; Yang S.J.; Ma, J.X.; He, Z.J.(2004): The construction of wavelet finite element and its application. *Finite Elements Analysis and Design*, vol.40, pp. 541-554.

Chen ,X.F.; Zi, Y.Y.; Li, B.; He, Z.J.(2006): Identification of multiple cracks using a dynamic mesh-refinement method. *The Journal of Strain Analysis for Engineering Design*, vol. 41 , pp. 31-39.

Diaz, L. A.; Martin, M.T.; Vampa, V. (2009): Daubechies wavelet beam and plate finite elements. *Finite Elements in Analysis and Design*, vol. 45, pp. 200-209.

Dilena, M.; Morassi, A.(2009): Structural health monitoring of rods based on natural frequency and antiresonant frequency measurements. *Structural Health Monitoring-An International Journal*, vol.8, pp. 149-173.

Dilena, M.; Morassi, A.(2010): Reconstruction method for damage detection in beams based on natural frequency and antiresonant frequency measurements. *Journal of Engineering Mechanics-ASCE*, vol. 136, pp. 329-344.

Dimarogonas,A.D.(1996): Vibration of cracked structures: a state of the art review. *Engineering Fracture Mechanics*, vol. 55 , pp. 831-854.

Doebling ,S.W. ; Farrar, C.R.; Prime,M.B. (1998): A summary review of vibration-based damage identification, The Shock and Vibration Digest **30** , pp. 91-105.

Han J.G., Ren W.X., Huang Y.(2006): A spline wavelet finite-element method in structural mechanics. *International Journal for Numerical Methods in Engineering*, vol.66, pp.166-190.

Han J.G., Ren W.X., Huang Y.(2007): A wavelet-based stochastic finite element method of thin plate bending. *Applied Mathematical Modelling*, vol.31, pp. 181-193.

Han J.G., Ren W.X., Huang Y.(2009): A spline wavelet finite element formulation of thin plate bending. *Engineering with Computers*, vol. 25, pp. 319-326.

He ,Y.Y.; Guo,D.; Chu,F.L. (2001): Using genetic algorithms and finite element methods to detect shaft crack for rotor-bearing system. *Mathematics and Computers in Simulation*. vol. 57, pp. 95-108.

Jia, R.Q.; Liu, S.T.(2006): Wavelet bases of Hermite cubic splines on the interval. *Advances in Computational Mathematics*, vol. 25 , pp. 23-39.

Khiem, N.T.;Lien, T.V.(2004): Multi-crack detection for beam by the natural frequencies. *Journal of Sound and Vibration*, vol. 273, pp. 175-184.

Lee,J.J.; Lee,J.W.; Yi,J.H.; Yun, C.B.; Jung,H.Y.(2005): Neural networks-based damage detection for bridges considering errors in baseline finite element models, *Journal of Sound and Vibration*, vol. 280 , pp. 555-578.

Lee,J.H.(2009a): Identification of multiple cracks in a beam using natural frequencies. *Journal of Sound and Vibration*, vol. 320, pp. 482-490.

Lee, J.H.(2009b): Identification of multiple cracks in a beam using vibration amplitudes. *Journal of Sound and Vibration*, vol.326, pp. 205-212.

Libre, N.A.; Emdadi, A.; Kansa, E.J.; Shekarchi, M.; Rahimian, M.(2008): A Fast Adaptive Wavelet scheme in RBF Collocation for nearly singular potential PDEs. *Computer Modeling in Engineering and Sciences*, vol.38, pp. 263-284.

Libre, N.A.; Emdadi, A.; Kansa, E.J.; Shekarchi, M.; Rahimian, M. (2009): Wavelet based adaptive RBF method for nearly singular potential-type problems on irregular domains. *CMES: Computer Modeling in Engineering and Sciences*, vol. 50, pp. 161-190.

Liu,S.W.; Huang,J.H.; Sung, J.C.; Lee, C.C.(2002): Detection of cracks using neural networks and computational mechanics. *Computer Methods in Applied Mechanics and Engineering*, vol. 191, pp. 2831-2845.

Ma, J.X.; Xue, J.J.; Yang S.J.; He, Z.J.(2003): A study of the construction and application of a Daubechies wavelet-based beam element. *Finite Elements Analysis and Design* , vol. 39, pp.965-975.

Montalvão ,D.; Maia, N.M.M.; Ribeiro,A.M.R.(2006): A review of vibration-based structural health monitoring with special emphasis on composite materials. *The Shock and Vibration Digest*, vol. 38, pp. 1-30.

Morassi,A.(2007): Damage detection and generalized Fourier coefficients. *Journal of Sound and Vibraion*, vol. 302, pp. 229-259.

Owolabi,G.M.; Swamidas, A.S.J.; Seshadri,R.(2003): Crack detection in beams using changes in frequencies and amplitudes of frequency response functions. *Journal of Sound and Vibration*, vol. 265, pp. 1-22.

Patil, D.P.; Maiti, S.K.(2003): Detection of multiple cracks using frequency measurements. *Engineering Fracture Mechanics*, vol.70, pp. 1553-1572.

Perera, R.; Ruiz, A. (2008): A multistage FE updating procedure for damage identification in large-scale structures based on multiobjective evolutionary optimization. *Mechanical System and Signal Processing*, vol. 22 , pp. 970-991.

Sekhar,A.S.(2008): Multiple cracks effects and identification. *Mechanical Systems and Signal Processing*, vol. 22, pp. 845-878.

Tada,H.; Paris, P.C.; Irwin,G.R.(2000): *The Stress Analysis of Cracks Handbook* (Third Edition). New York, The American Society of Mechanical Engineers.

Vampa, V.; Martin, M.T., Serrano, E. (2010): A hybrid method using wavelets for the numerical solution of boundary value problems on the interval. *Applied Mathematics and Computation*, vol. 217, pp. 3355-3367.

Wauer,J.(1990): Dynamics of cracked rotors:literature survey. *Applied Mechanics Reviews*, vol. 43 , pp. 13-17.

Wu,X.; Ghaboussi,J.; Gaarrett,J.H.(1992): Use of neural networks in detection of structural damage. *Computers and Structures*, vol. 42, pp. 649-659.

Xiang, J.W.; Chen,X. F.; He Y. M.; He,Z.J.(2006): Identification of crack in a beam based on finite element method of B-spline wavelet on the interval. *Journal of Sound and Vibration*, vol. 296, pp. 1046-1052.

Xiang,J.W.; Chen, X. F.; He, Y. M.; He,Z.J.(2007): Identification of crack in a rotor system based on wavelet finite element method. *Finite Elements in Analysis and Design*, vol. 43, pp. 1068-1081.

Xiang ,J.W.; Zhong,Y. T.; Chen,X.F.; He,Z.J.(2008a): Crack Detection in a Shaft by Combination of the New Wavelet-based Elements and Genetic Algorithm. *International Journal of Solids and Structures*, vol. 45, pp. 4782-4795.

Xiang, J.W., Chen, X.F., Yang L.F. and He, Z.J.(2008b): A Class of Wavelet-based Flat Elements Using B-spline Wavelet on the Interval and Its applications. *CMES: Computer Modeling in Engineering and Sciences*, vol.23, pp.1-12.

Yan, Z.Z.; Wang, Y.S.; Zhang C.Z.(2008): A method based on wavelets for band structure analysis of phononic crystals. *CMES: Computer Modeling in Engineering and Sciences*, vol. 38, pp.59-88.

Yuan, S.F.; Wang,L.; Peng, G.(2005): Neural network method based on a new damage signature for structural health monitoring. *Thin-Walled Structures*, vol. 43, pp. 553-563.

Zachiarias,J.; Hartmann, C.; Delgado, A. (2004): Damage detection on crates of beverages by artificial neural networks trained with finite-element data. *Computer methods in applied mechanics and engineering*, vol. 193, pp. 561-574.

Zhou Y.H., Zhou J.(2008a): A modified wavelet approximation of deflections for solving PDEs of beams and square thin plates. *Finite Elements in Analysis and Design*, vol. 44, 773-783.

Zhou Y.H., Zhou J.(2008b): A modified wavelet approximation for multi-resolution AWCM in simulating nonlinear vibration of MDOF systems .*Computer Methods in Applied Mechanics and Engineering*, vol.197, pp.1466-1478.